*Research Article*

# Shielding Characteristics of Polydimethylsiloxane Reinforced with Iron for Radiation Protection

Enayatolah Yazdankish[a1]

[a]Applied Chemistry Department, Faculty of Gas and Petroleum, Yasouj University, Gachsaran 75813-56001, Iran

## Abstract

This study investigates the radiation-shielding properties of polydimethylsiloxane reinforced with iron in weight fractions ranging from 5% to 40%. The density of the composite material was calculated using a formula that considers the densities of Polydimethylsiloxane and iron. The mass attenuation coefficient, linear attenuation coefficient, half-value layer, effective atomic number, and equivalent atomic number were calculated using the WinXCom program. The results indicated that the mass attenuation and linear attenuation coefficient values were higher for low-energy photons, and the composites reinforced with higher weights of iron displayed higher mass attenuation and linear attenuation coefficients. The contribution of Compton scattering remains almost constant across the energy range, while the photoelectric effect dominates at low energies, and pair production becomes increasingly dominant at higher energies. The half-value layer decreased as the weight fraction of iron in the composite increased, making composites with a higher weight fraction more efficient at attenuating radiation to a certain level. The effective atomic number and equivalent atomic number values were also higher for composites with a higher weight fraction of iron, indicating that they are more effective at attenuating radiation. Overall, Polydimethylsiloxane reinforced with iron shows promise as a material for radiation shielding applications.

**Keywords:** Mass Attenuation Coefficient; Radiation Protection; Shielding Characteristics; Polydimethylsiloxane Polymer.

## 1. Introduction

Exposure to ionizing radiation can pose a significant health risk, making proper shielding equipment essential when handling radioactive materials [1-3]. Shielding materials can significantly reduce the risk and minimize the hazards of ionizing radiation. Traditionally, materials such as concrete and lead have been used for shielding, but they have limitations and drawbacks. For example, lead is toxic, has a low melting point, and can leak radiation due to heat generated with long exposure [4, 5]. Concrete is prone to cracking and loss of moisture, which can reduce its absorption efficiency and increase radiation leakage.

In recent years, research has been conducted to investigate the effectiveness of other materials for shielding against ionizing radiation, including modified concrete, polymers,

[1] enayat.yazdankish@gmail.com



[ Downloaded from jgp.yu.ac.ir on 2026-10-05 ]

composite materials, glasses, metallic alloys, stainless steels, and ceramics. These materials have been evaluated for suitability as shielding materials in various applications. The ideal shielding material should have high shielding effectiveness, be cost-effective, readily available, and easy to handle [6].

The development of new and improved shielding materials is an ongoing area of research in radiation protection and dosimetry. Advanced materials, such as nanocomposites and metamaterials, are being explored for their potential to provide superior radiation-shielding properties [7, 8]. Using these innovative materials could lead to improved radiation protection and dosimetry for various applications.

Overall, selecting appropriate shielding material is critical for minimizing the risk of ionizing radiation hazards. While traditional materials such as concrete and lead have been widely used for shielding, new and innovative materials are being developed to provide better radiation protection. The use of advanced materials will not only improve the safety of individuals working with radioactive materials, but it will also help to minimize the potential for environmental damage from radiation exposure. Ongoing research and development are crucial to ensure that the most effective and efficient shielding materials are available for radiation protection and dosimetry.

Polydimethylsiloxane (PDMS) has attracted significant attention as a radiation shielding material due to its high hydrogen content (hydrogen is the best nucleus in absorbing the energy of energetic neutrons.) and unique properties, including high flexibility, low toxicity, and biocompatibility. However, the low atomic number (Z) of PDMS limits its effectiveness in blocking higher-energy radiation such as gamma rays. To address this limitation, researchers have investigated using PDMS reinforced with heavy particles as a composite material for radiation shielding. The addition of heavy particles to PDMS increases its atomic number, enhancing its ability to attenuate higher-energy radiation. PDMS-metal composites have been shown to have promising radiation attenuation properties for various applications, including medical radiation therapy and nuclear power plants. However, further research is needed to optimize the properties of PDMS composites and evaluate their long-term durability and stability under exposure to ionizing radiation [9, 10]. In this study, we investigate PDMS-Fe composites' radiation shielding properties and mechanical stability for potential use in radiation protection applications.

X-rays and gamma rays are ionizing radiation that interacts with matter through the absorption, scattering, and ionization of atoms and molecules[11, 12]. When X-rays or gamma rays pass through matter, they can be absorbed by the atoms and molecules in the material, leading to the ejection of electrons and the production of ion pairs. The probability of absorption depends on the energy of the radiation and the atomic number (Z) of the material[13, 14].

The interaction of photons with matter can be described by the photoelectric effect, Compton scattering, and pair production [15-17]. In the photoelectric effect, an atom or molecule absorbs a photon, and an electron is ejected from the atom or molecule [18]. This process occurs when the photon's energy is equal to or greater than the electron's binding energy in the atom or molecule. In Compton scattering,



[ Downloaded from jgp.yu.ac.ir on 2026-10-05 ]

a photon collides with an electron in the material, transferring some of its energy to the electron and causing it to recoil. The scattered photon has less energy and a longer wavelength than the original. Compton scattering is the dominant process for intermediate-energy photons. In pair production, a high-energy photon interacts with the electric field of a nucleus and is converted into an electron-positron pair. The energy of the photon must be at least twice the rest mass of an electron to produce a pair. Pair production is the dominant process for very high-energy photons [19].

Understanding the interaction of radiation with matter is essential for many applications, including radiation therapy, nuclear power, and radiation protection, and ongoing research is needed to improve our understanding of these interactions and develop more effective radiation shielding materials and strategies. This study represents a novel contribution to the field of radiation shielding materials by investigating the radiation shielding properties of polydimethylsiloxane reinforced with iron across a range of weight fractions. By calculating key parameters such as the mass attenuation coefficient, linear attenuation coefficient, half-value layer, effective atomic number, and equivalent atomic number using the WinXCom program, this research sheds light on the behavior of these composite materials in attenuating radiation. In the subsequent section, we will provide a comprehensive theoretical description of the photon-matter interaction phenomenon, elucidating the fundamental principles governing the interaction between photons and the composite material under investigation. This section will cover the mechanisms of photon absorption, scattering, and transmission, and their respective contributions to the attenuation of radiation. In section 3, we will present the results of our calculations, which will be based on the theoretical framework presented in the previous section. These calculations will involve the determination of various parameters such as the mass attenuation coefficient, linear attenuation coefficient, half-value layer, effective atomic number, and equivalent atomic number, which are essential for evaluating the radiation shielding capabilities of the composite material. The results will be presented clearly and concisely, and their implications will be discussed in the context of potential practical applications.

## 2. Theory

Polydimethylsiloxane (PDMS), a silicon-based organic polymer is, widely used in various industries due to its unique properties, such as high thermal stability, chemical inertness, low toxicity, and excellent mechanical properties. PDMS has several biomedical properties that make it useful for various applications in the biomedical field. These properties include biocompatibility, low toxicity, flexibility and elasticity, optical transparency, low protein binding, and thermal stability. The biomedical properties of PDMS make it a versatile material that can be used in a wide range of biomedical applications, including medical devices, microfluidics, biosensors, and tissue engineering. PDMS has been used to develop radiation shielding materials to minimize the risk of ionizing radiation hazards. Ionizing radiation can cause damage to living tissue by ionizing the atoms and molecules in the tissue, which can lead to mutations and cell death. Therefore, it is



[ Downloaded from jgp.yu.ac.ir on 2026-10-05 ]

important to develop effective shielding materials to protect individuals from exposure to ionizing radiation. PDMS is a suitable material for radiation shielding because of its high hydrogen content and low atomic number, which makes it an effective shield against low-energy radiation, such as gamma and X-rays. PDMS can be used to coat or add an additive to radiation shielding materials, such as concrete, to improve their radiation attenuation properties. In one study [3], PDMS was added to concrete to create a composite material effective at attenuating gamma radiation. The PDMS improved the hydrogen content of the concrete, which increased its ability to absorb gamma rays. The composite material effectively reduced the radiation dose rate and shielded against gamma radiation. PDMS can also be used to develop personal protective equipment (PPE) for radiation workers. For example, PDMS can coat gloves and other protective gear to improve their radiation-shielding properties. PDMS-coated gloves have been shown to provide effective shielding against gamma radiation, reducing the dose rate to the hands of the wearer. Overall, PDMS has shown promise as a material for radiation shielding in various applications, including in developing shielding materials and personal protective equipment.

In this study, we aimed to investigate the behavior of radiation in different reinforced composites of PDMS by generating mass attenuation coefficients (MAC) and photon interaction cross-sections using the WinXCom program [20]. The MAC values represent the amount of radiation absorbed by a material, and they were calculated for a range of energies between 0.015 MeV to 15 MeV. The interaction between photons and matter encompasses a variety of phenomena, including Rayleigh scattering, the photoelectric effect, Compton scattering, and pair production. Each of these interactions is characterized by its unique physics and cross-sections, which depend on the energy of the photons. Specifically, at low photon energies, Rayleigh scattering is the dominant interaction mechanism, whereas, at high energies, pair production becomes the dominant process.

Rayleigh scattering is a phenomenon in which light is scattered by particles along its path that are smaller in size than one-tenth the wavelength of the light. This type of scattering occurs without any loss of energy or change in wavelength. One of the most well-known applications of Rayleigh scattering is explaining the blue color of the sky, but it has many other useful applications as well [14]. The validity of Rayleigh scattering is determined by the size of the scattering particle, defined as, $x = 2\pi r/\lambda$ , with $r$ the radius of the particle and λ the wavelength of the light, being much smaller than one. In the range where Rayleigh scattering takes place, the intensity of the scattered light can be expressed using the following formula [21].

$$I = I_0 \frac{1+\cos^2\theta}{2R^2}\left(\frac{2\pi}{\lambda}\right)^4\left(\frac{n^2-1}{n^2+2}\right)^2\left(\frac{d}{2}\right)^6 \qquad (1)$$

Here, $I_0$ represents the intensity of the incident light, $\theta$ denotes the scattering angle, λ represents the wavelength of light, $R$ refers to the distance from the particle, $n$ is the refractive index, and $d$ represents the diameter of the scattering particle.

The photoelectric effect is a physical phenomenon in which the absorption of light by a metal surface results in the ejection of electrons from the metal. The occurrence of the photoelectric effect requires that the energy carried by the incident photons is sufficient to



[ Downloaded from jgp.yu.ac.ir on 2026-10-05 ]

overcome the attractive forces that bind the electrons to the nuclei of the metal atoms. This minimum required energy for electron ejection is called the threshold energy. For low energies (The ratio of photon energy to electron rest state energy be less than 0.9), the cross-section of the photoelectric effect can be approximated by the simplified equation of [22]:

$$\sigma_{ph} \approx 3\times10^{12}\frac{Z^4}{E^{3.5}} \quad (2)$$

where Z is the atomic number of the target and E is the incident photon energy.

Compton scattering is a fundamental interaction between photons and electrons, which occurs when a photon collides with an outer orbital electron. During this interaction, the incident photon transfers some of its energy to the electron, causing it to recoil and be ejected from its original position. The scattered photon's trajectory is altered, moving from the collision site in a new direction. The energy of the scattered photon is reduced by an amount equal to the kinetic energy gained by the recoiling electron and its binding energy. Compton scattering can lead to the ionization of the absorbing atom, resulting in the loss of an electron. It is a crucial process in X-ray and gamma-ray spectroscopy, as it enables the determination of the energy and direction of the scattered photons, which can provide valuable insights into the properties of the material being studied.

In high-energy photons with energies in the MeV range or greater, pair production is the primary mode of interaction with matter. When a high-energy photon approaches an atomic nucleus, it can be converted into an electron-positron pair, where the photon's energy is transformed into particle mass by Einstein's equation, $E = mc^2$ . For pair production to occur, the photon must possess energy greater than the sum of the rest mass energies of an electron and positron (2.511 KeV=1.022 MeV), corresponding to a photon wavelength of 1.2132 Pico meters. The production of an electron-positron pair requires the mediation of a nucleus, which absorbs the excess momentum, and the liberated pair is subject to further interactions with matter. Pair production is a crucial process in high-energy physics, astrophysics, and medical physics, as it enables detecting and studying high-energy photons and provides insights into the structure and composition of matter.

The Beer-Lambert law (Eq. (3)) is used to determine the mass attenuation coefficient ( $\mu/\rho$ ) of a material by measuring the intensity (I) of a mono-energetic photon transmitted through a layer of the material with a thickness of x and comparing it to the incident intensity ($I_0$) [23, 24]. In addition to the MAC, the total linear attenuation coefficient (μ) was computed to understand better how radiation interacts with materials. The μ value is obtained by multiplying the material's density by its MAC and represents the probability of a photon interacting with the material as it passes through it. This value is essential for calculating other radiation-related quantities, such as the Half Value Layer (HVL) and Tenth Value Layer (TVL).

$$I = I_0 e^{(\mu/\rho)\rho x} \quad (3)$$

The HVL represents the thickness of a material that reduces the radiation level by half, and it is calculated by dividing 0.693 by the linear attenuation coefficient. The TVL, on the other hand, represents the thickness of a material that attenuates a radiation beam to 10% of its initial level, and it is calculated by dividing 2.303 by



[ Downloaded from jgp.yu.ac.ir on 2026-10-05 ]

the linear attenuation coefficient. These parameters are useful in determining the effectiveness of different materials in shielding against radiation. The mean free path or relaxation length (λ) is also calculated, representing the average distance between two successive interactions of photons with the material. The λ value is determined by dividing one by the linear attenuation coefficient and is an important parameter in understanding how radiation interacts with materials. These parameters provide valuable insights into the behavior of radiation in different materials and can be used to design and optimize radiation shielding materials [25].

Effective atomic numbers ($Z_{eff}$) and effective electron densities ($N_{eff}$) are important parameters in determining the penetration rate of X and gamma photons in materials that contain multiple elements. Numerous studies have been conducted on $Z_{eff}$ and $N_{eff}$ for various structures such as biological materials, alloys, compounds, glass, and minerals. In the energy region where photon interactions occur, it is challenging to express the number of atoms in a compound, alloy, glass, mineral structure, or biological material as a single quantity. To overcome this issue, Hine proposed a method to calculate $Z_{eff}$ that considered the atomic number of all constituent elements in the material. $Z_{eff}$ and $N_{eff}$ values provide information on the scattering and absorption of total cross-sections of gamma rays in a given energy range. $Z_{eff}$ is calculated using the mass attenuation coefficient values for the absorbed photons and varies with energy. Interestingly, $Z_{eff}$ values may change without being dependent on the photon energy in the intermediate energy range.

The effective atomic number of composite materials ( $Z_{eff}$ ) is the equivalent atomic number of a composite material that produces the same effect as a single element when interacting with photons. This parameter is determined by the ratio of the atomic cross-section to the electronic cross-section and is useful in understanding how different materials interact with radiation. The effective atomic number is given by [23, 26]:

$$Z_{eff} = \frac{\sigma_a}{\sigma_e} = \frac{\sum_i f_i A_i (\mu/\rho)_i}{\sum_i f_i (A_i/Z_i)(\mu/\rho)_i} \qquad (4)$$

Where, $\sigma_a$ and $\sigma_e$ are atomic cross-section and electronic cross-section respectively, $A_i$, $Z_i$, and $f_i$ are mass number, atomic number, and weight fraction of the ith element in molecule or composite.

The effective electron density ( $N_{eff}$ ) is a parameter that is related to the effective atomic number of a material. It is defined as the number of electrons per unit mass and can be expressed mathematically using the following equation [27, 28]:

$$N_{eff} = \frac{N}{\langle A \rangle} Z_{eff} \qquad (5)$$

where $\langle A \rangle$ and $N$ is the average atomic mass of the composite and Avogadro constant respectively. The radiation protection efficiency RPE of a composite material is determined by its ability to attenuate ionizing radiation, and is determined as follows [29, 30]:

$$RPE = \left(1 - \frac{I}{I_0}\right) \times 100 \qquad (6)$$



[ Downloaded from jgp.yu.ac.ir on 2026-10-05 ]

## 3. Results

PDMS was selected as the base material and reinforced with iron in five different weight fractions, namely Fe-5%, Fe-10%, Fe-20%, Fe-30%, and Fe-40%. In the literature, some references used or made a composite with a 40% or higher weight fraction of iron [31]. The density of PDMS is 0.996 g/cm$^3$, and that of iron is 7.874 g/cm$^3$. To calculate the density of the composite material, the following formula was utilized:zwhere, $\rho$, $\rho_p$, $\rho_F$, $w_P$, and $w_F$ represent the density of the composite, the density of PDMS, the density of iron, the weight fraction of PDMS, and the weight fraction of iron, respectively. Using this equation, we can calculate the density of the composite at weight fractions of iron ranging from 5% to 40%, resulting in values of 1.013, 1.058, 1.170, 1.310, and 1.487 $g/cm^3$, respectively.

In the preceding section, we expounded upon Rayleigh scattering; however, this type of photon interaction with matter does not significantly impact our calculations. This is because atoms are on the order of some angstrom in size, as previously mentioned, and the corresponding wavelength must exceed a nanometer, which results in an energy of less than 1 KeV. This energy level is considerably less than the values we have taken into account. The considered energy of the incident photon varies from 0.015 to 15 MeV (the wavelength of 0.82 to $0.82 \times 10^{-3}$ Angstrom) therefore the chemical bounds, the cross-link density, the size of the additive iron, and other chemical properties (except atomic number and density) do not affect damping attenuation coefficient.

The key characteristic of a radiation shielding material is its mass attenuation coefficient, which is dependent on the cross-sections of the photoelectric effect, Compton scattering, and pair production. In this study, the MAC was calculated using the WinXCom program [20]. Table 1 presents the MAC and LAC as a function of energy for various types of PDMS composites reinforced with different weights of iron. The results indicate that the MAC and LAC values are higher for low-energy photons than for high-energy photons. Furthermore, the composites reinforced with higher weights of iron display higher MAC and LAC coefficients, as evidenced by the data.

***Table 1***. *Mass Attenuation Coefficient and Linear Attenuation Coefficient as a Function of Energy for Five PDMS Composites Reinforced with Varying Weights of Iron.*

| Energy MeV | Fe-5% | | Fe-10% | | Fe-20% | | Fe-30% | | Fe-40% | |
|---|---|---|---|---|---|---|---|---|---|---|
| | MAC(cm$^2$/g) | LAC(1/cm) | MAC(cm$^2$/g) | LAC(1/cm) | MAC(cm$^2$/g) | LAC(1/cm) | MAC(cm$^2$/g) | LAC(1/cm) | MAC(cm$^2$/g) | LAC(1/cm) |
| 1.50E-02 | 7.23E+00 | 7.32E+00 | 9.85E+00 | 1.04E+01 | 1.51E+01 | 1.77E+01 | 2.03E+01 | 2.67E+01 | 2.56E+01 | 3.81E+01 |
| 1.00E-01 | 1.86E-01 | 1.88E-01 | 1.96E-01 | 2.07E-01 | 2.15E-01 | 2.52E-01 | 2.35E-01 | 3.07E-01 | 2.54E-01 | 3.78E-01 |
| 3.00E-01 | 1.15E-01 | 1.17E-01 | 1.15E-01 | 1.22E-01 | 1.15E-01 | 1.34E-01 | 1.14E-01 | 1.49E-01 | 1.13E-01 | 1.69E-01 |
| 6.62E-01 | 8.29E-02 | 8.40E-02 | 8.24E-02 | 8.72E-02 | 8.14E-02 | 9.53E-02 | 8.04E-02 | 1.05E-01 | 7.94E-02 | 1.18E-01 |
| 8.00E-01 | 7.60E-02 | 7.70E-02 | 7.55E-02 | 7.99E-02 | 7.46E-02 | 8.72E-02 | 7.36E-02 | 9.64E-02 | 7.27E-02 | 1.08E-01 |
| 1.17E+00 | 6.31E-02 | 6.39E-02 | 6.27E-02 | 6.63E-02 | 6.18E-02 | 7.24E-02 | 6.10E-02 | 7.99E-02 | 6.02E-02 | 8.95E-02 |
| 1.33E+00 | 5.91E-02 | 5.99E-02 | 5.87E-02 | 6.21E-02 | 5.79E-02 | 6.78E-02 | 5.72E-02 | 7.49E-02 | 5.64E-02 | 8.39E-02 |
| 1.50E+00 | 5.56E-02 | 5.63E-02 | 5.52E-02 | 5.84E-02 | 5.45E-02 | 6.38E-02 | 5.38E-02 | 7.05E-02 | 5.31E-02 | 7.90E-02 |
| 2.51E+00 | 4.25E-02 | 4.31E-02 | 4.23E-02 | 4.48E-02 | 4.19E-02 | 4.90E-02 | 4.15E-02 | 5.44E-02 | 4.11E-02 | 6.12E-02 |



[ Downloaded from jgp.yu.ac.ir on 2026-10-05 ]

| Energy MeV | Fe-5% | | Fe-10% | | Fe-20% | | Fe-30% | | Fe-40% | |
|---|---|---|---|---|---|---|---|---|---|---|
| | MAC($cm^2/g$) | LAC(1/cm) | MAC($cm^2/g$) | LAC(1/cm) | MAC($cm^2/g$) | LAC(1/cm) | MAC($cm^2/g$) | LAC(1/cm) | MAC($cm^2/g$) | LAC(1/cm) |
| 5.00E+00 | 3.02E-02 | 3.06E-02 | 3.02E-02 | 3.20E-02 | 3.04E-02 | 3.55E-02 | 3.05E-02 | 4.00E-02 | 3.06E-02 | 4.56E-02 |
| 8.00E+00 | 2.49E-02 | 2.52E-02 | 2.52E-02 | 2.66E-02 | 2.57E-02 | 3.01E-02 | 2.62E-02 | 3.44E-02 | 2.68E-02 | 3.98E-02 |
| 1.00E+01 | 2.32E-02 | 2.35E-02 | 2.35E-02 | 2.49E-02 | 2.42E-02 | 2.84E-02 | 2.50E-02 | 3.27E-02 | 2.57E-02 | 3.82E-02 |
| 1.50E+01 | 2.10E-02 | 2.13E-02 | 2.15E-02 | 2.28E-02 | 2.26E-02 | 2.64E-02 | 2.36E-02 | 3.10E-02 | 2.47E-02 | 3.67E-02 |

Table 2 displays the effective atomic number and effective electron density values. The $Z_{eff}$ and $N_{eff}$ values exhibit a decreasing trend as the energy increases, except for a notable increase at approximately 15 MeV. Additionally, the data indicate that composites reinforced with higher weights of iron exhibit higher $Z_{eff}$ and $N_{eff}$ coefficients.

***Table 2.*** *Variation of Effective Atomic Number and Effective Electron Density with Energy for Five Different PDMS Composites Reinforced with Varying Weights of Iron.*

| Energy MeV | Fe-5% | | Fe-10% | | Fe-20% | | Fe-30% | | Fe-40% | |
|---|---|---|---|---|---|---|---|---|---|---|
| | $Z_{eff}$ | $N_{eff}$ ($\times10^{23}$) | $Z_{eff}$ | $N_{eff}$ ($\times10^{23}$) | $Z_{eff}$ | $N_{eff}$ ($\times10^{23}$) | $Z_{eff}$ | $N_{eff}$ ($\times10^{23}$) | $Z_{eff}$ | $N_{eff}$ ($\times10^{23}$) |
| 1.50E-02 | 14.6615 | 11.3546 | 16.911 | 12.5034 | 19.8221 | 13.2648 | 21.624 | 12.9533 | 22.8494 | 12.084 |
| 1.00E-01 | 4.6595 | 3.6086 | 5.0764 | 3.7533 | 6.0042 | 4.018 | 7.0827 | 4.2427 | 8.3518 | 4.4169 |
| 3.00E-01 | 4.2025 | 3.2546 | 4.3872 | 3.2437 | 4.8135 | 3.2212 | 5.3376 | 3.1974 | 5.9973 | 3.1717 |
| 6.62E-01 | 4.1747 | 3.2331 | 4.3459 | 3.2132 | 4.742 | 3.1733 | 5.2305 | 3.1332 | 5.8479 | 3.0927 |
| 8.00E-01 | 4.1699 | 3.2294 | 4.3401 | 3.2089 | 4.7337 | 3.1678 | 5.2193 | 3.1265 | 5.8333 | 3.085 |
| 1.17E+00 | 4.1618 | 3.2231 | 4.3308 | 3.202 | 4.7218 | 3.1598 | 5.2042 | 3.1174 | 5.8144 | 3.075 |
| 1.33E+00 | 4.1744 | 3.2329 | 4.3438 | 3.2116 | 4.7356 | 3.169 | 5.2191 | 3.1264 | 5.8305 | 3.0835 |
| 1.50E+00 | 4.1715 | 3.2306 | 4.3411 | 3.2097 | 4.7335 | 3.1676 | 5.2176 | 3.1254 | 5.8297 | 3.0831 |
| 2.51E+00 | 4.2222 | 3.2699 | 4.4001 | 3.2533 | 4.8111 | 3.2196 | 5.3171 | 3.1851 | 5.9554 | 3.1496 |
| 5.00E+00 | 4.4277 | 3.429 | 4.6384 | 3.4295 | 5.1227 | 3.4281 | 5.7141 | 3.4229 | 6.4523 | 3.4123 |
| 8.00E+00 | 4.7096 | 3.6473 | 4.9637 | 3.67 | 5.5435 | 3.7097 | 6.2437 | 3.7401 | 7.1059 | 3.758 |
| 1.00E+01 | 4.8919 | 3.7885 | 5.173 | 3.8248 | 5.8117 | 3.8892 | 6.5776 | 3.9401 | 7.5126 | 3.9731 |
| 1.50E+01 | 5.2947 | 4.1005 | 5.6337 | 4.1654 | 6.3958 | 4.28 | 7.2957 | 4.3703 | 8.3745 | 4.4289 |

Table 3 presents two critical parameters involved in the fabrication of radiation shielding, namely the half-value layer and tenth value layer. The HVL and TVL values are low for low-energy photons but increase with increasing photon energy. In addition, the data reveal that composites with higher weight fractions of iron exhibit lower thickness values for both HVL and TVL.

***Table 3.*** *Half Value Layer and Tenth Value Layer of Incoming Beam for Five Types of PDMS Composites Reinforced with Varying Weights of Iron.*

| Energy MeV | Fe-5% | | Fe-10% | | Fe-20% | | Fe-30% | | Fe-40% | |
|---|---|---|---|---|---|---|---|---|---|---|
| | HVL(cm) | TVL (cm) | HVL(cm) | TVL (cm) | HVL (cm) | TVL (cm) | HVL (cm) | TVL (cm) | HVL (cm) | TVL (cm) |
| 1.50E-02 | 0.0947 | 0.3146 | 0.0665 | 0.2209 | 0.0392 | 0.1303 | 0.026 | 0.0864 | 0.0182 | 0.0605 |
| 1.00E-01 | 3.6842 | 12.2385 | 3.3509 | 11.1313 | 2.7543 | 9.1497 | 2.2548 | 7.4901 | 1.8334 | 6.0905 |



[ Downloaded from jgp.yu.ac.ir on 2026-10-05 ]

| Energy MeV | Fe-5% | | Fe-10% | | Fe-20% | | Fe-30% | | Fe-40% | |
|---|---|---|---|---|---|---|---|---|---|---|
| | HVL(cm) | TVL (cm) | HVL(cm) | TVL (cm) | HVL (cm) | TVL (cm) | HVL (cm) | TVL (cm) | HVL (cm) | TVL (cm) |
| 3.00E-01 | 5.9253 | 19.6835 | 5.6878 | 18.8943 | 5.1696 | 17.1732 | 4.641 | 15.4169 | 4.1097 | 13.6521 |
| 6.62E-01 | 8.2529 | 27.4157 | 7.9494 | 26.4073 | 7.2759 | 24.1699 | 6.5783 | 21.8527 | 5.8676 | 19.4916 |
| 8.00E-01 | 9.0048 | 29.9133 | 8.6759 | 28.8206 | 7.945 | 26.3927 | 7.1872 | 23.8754 | 6.4142 | 21.3076 |
| 1.17E+00 | 10.8487 | 36.0387 | 10.4551 | 34.7311 | 9.5793 | 31.8219 | 8.6703 | 28.8021 | 7.742 | 25.7185 |
| 1.33E+00 | 11.5805 | 38.4695 | 11.1603 | 37.0739 | 10.2256 | 33.9688 | 9.2553 | 30.7456 | 8.2645 | 27.4542 |
| 1.50E+00 | 12.3089 | 40.8892 | 11.8613 | 39.4022 | 10.8658 | 36.0954 | 9.8329 | 32.6642 | 8.7786 | 29.1618 |
| 2.51E+00 | 16.0972 | 53.4737 | 15.4836 | 51.4354 | 14.1317 | 46.9447 | 12.7401 | 42.3217 | 11.3301 | 37.6377 |
| 5.00E+00 | 22.6762 | 75.3286 | 21.6631 | 71.9633 | 19.5022 | 64.7848 | 17.3407 | 57.6047 | 15.2092 | 50.5239 |
| 8.00E+00 | 27.4597 | 91.2192 | 26.0175 | 86.4281 | 23.046 | 76.5572 | 20.1708 | 67.006 | 17.4209 | 57.871 |
| 1.00E+01 | 29.5189 | 98.0598 | 27.8361 | 92.4697 | 24.4328 | 81.164 | 21.1995 | 70.4234 | 18.1584 | 60.321 |
| 1.50E+01 | 32.5513 | 108.133 | 30.413 | 101.0297 | 26.2327 | 87.1431 | 22.3958 | 74.3974 | 18.8966 | 62.7731 |

The attenuation of radiation is closely associated with the cross-sections of the photoelectric effect, Compton scattering, and pair production. Figure 1 illustrates these effects for a 40% reinforced composite, revealing that the photoelectric effect dominates at low energies, while pair production becomes increasingly dominant at higher energies. Meanwhile, the contribution of Compton scattering remains almost constant across the energy range.

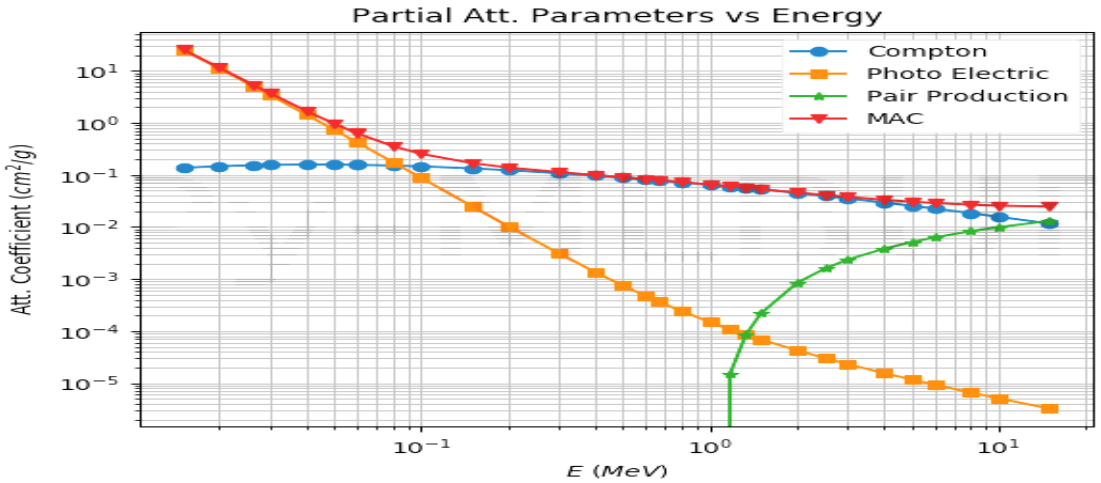


***Figure 1.*** *Partial attenuation coefficient of the photoelectric effect, Compton scattering, pair production, and the whole attenuation coefficient*

Figure 2, part (a), displays the mass attenuation coefficients plotted against energy for different iron-reinforced composites. The MAC measures how much a material attenuates or reduces the intensity of a beam of radiation as it passes through the material. In this case, the plot shows that the MAC increases as the weight fraction of iron in the composite increases. This means that composites with a higher weight fraction of iron will better attenuate radiation at a given energy level.



[ Downloaded from jgp.yu.ac.ir on 2026-10-05 ]

Part (b) of Figure 2, shows the plotted half-value layer, which measures the thickness of a material needed to reduce the intensity of a beam of radiation to half its initial value. As the weight fraction of iron in the composite increases, the HVL decreases. This means that composites with a higher weight fraction of iron require less material to attenuate radiation to a certain level, making them more efficient.

Part (c) of Figure 2 displays the plotted effective atomic number, which measures the average atomic number of the atoms in a material. Composites with a higher weight fraction of iron have a higher $Z_{eff}$, meaning that the average atomic number of the atoms in the composite is higher. This makes the composite more effective at attenuating radiation since higher atomic numbers increase the likelihood of interactions between the radiation and the atoms in the material.

Finally, part (d) of Figure 2 displays the plotted equivalent atomic number. To determine the equivalent atomic number of a material, the ratio $(\mu/\rho)Comp./(\mu/\rho)total$ at a given energy is compared to the corresponding ratio of a pure element at the same energy. The higher the weight fraction of iron in the composite, the higher the $Z_{eq}$. This means that composites with a higher weight fraction of iron have more electrons that are likely to interact with radiation, making them more effective at attenuating it.

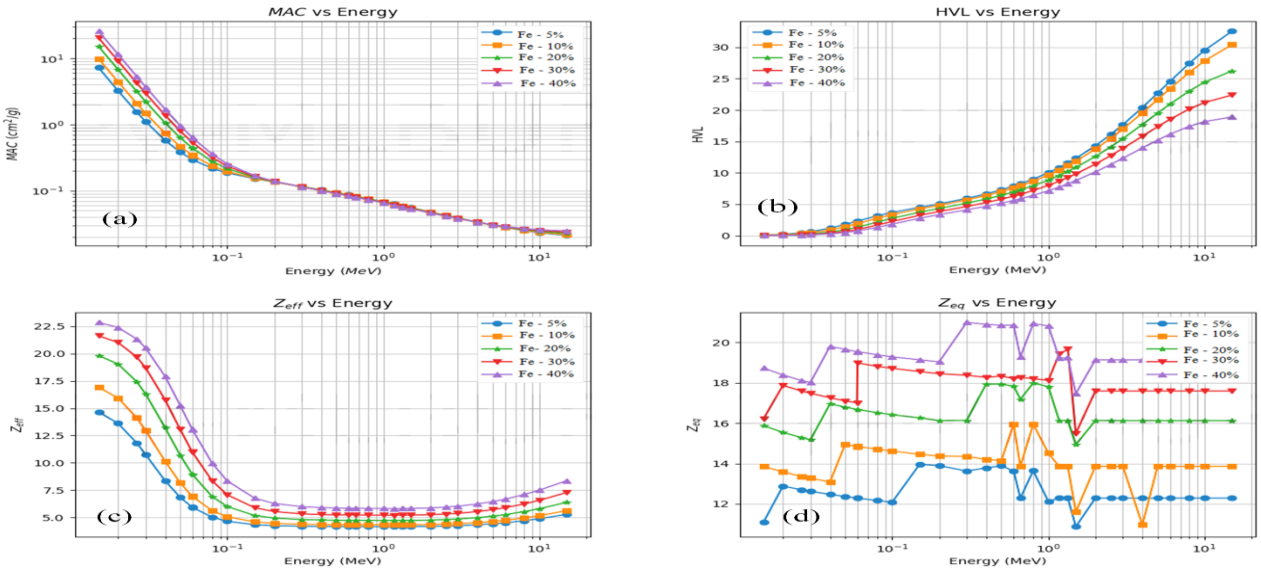


***Figure 2.*** *Part (a) displays the mass attenuation coefficients plotted against energy for different iron-reinforced composites. The MAC increases with a higher weight fraction of iron. Part (b) shows the plotted HVL, which decreases with an increase in weight fraction. Part (c) displays the plotted $Z_{eff}$, which is higher for composites with a greater weight fraction of iron. Finally, part (d) shows the $Z_{eq}$ plotted against weight fraction, with a higher weight fraction of iron resulting in a higher $Z_{eq}$.*

## 4. conclusion

In conclusion, the investigation into the radiation shielding properties of Polydimethylsiloxane reinforced with iron has demonstrated promising results for its application in radiation shielding. The study revealed that composites with higher weight fractions of iron exhibit increased mass attenuation and linear attenuation coefficients, indicating their enhanced ability to attenuate radiation. The findings also elucidated the



[ Downloaded from jgp.yu.ac.ir on 2026-10-05 ]

influence of iron content on key parameters such as the half-value layer, effective atomic number, and equivalent atomic number, further highlighting the efficacy of these composite materials in radiation attenuation. By identifying the dominance of different attenuation mechanisms at varying energy levels and the relationship between iron weight fraction and shielding efficiency, this research provides valuable insights for the development of superior radiation shielding materials. Overall, Polydimethylsiloxane reinforced with iron shows great promise as a viable option for enhancing radiation shielding capabilities in various applications.

## References


1. Lucas, J., et al., *Rapid translocation frequency analysis in humans decades after exposure to ionizing radiation.* International journal of radiation biology, 1992. **62**(1): p. 53-63.
2. Scanff, P., J. Donadieu, P. Pirard, and B. Aubert, *Population exposure to ionizing radiation from medical examinations in France.* The British journal of radiology, 2008. **81**(963): p. 204-213.
3. Yazdankish, E., M. Foroughi, and M.H.A. Azqhandi, *Capture of I131 from medical-based wastewater using the highly effective and recyclable adsorbent of g-C3N4 assembled with Mg-Co-Al-layered double hydroxide.* Journal of hazardous materials, 2020. **389**: p. 122151.
4. Godwin, H.A., *The biological chemistry of lead.* Current opinion in chemical biology, 2001. **5**(2): p. 223-227.
5. Charkiewicz, A.E. and J.R. Backstrand, *Lead toxicity and pollution in Poland.* International journal of environmental research and public health, 2020. **17**(12): p. 4385.
6. Bawazeer, O., et al., *A review on using nanocomposites as shielding materials against ionizing radiation.* Journal of Umm Al-Qura University for Applied Sciences, 2023. **9**(3): p. 325-340.
7. Rajavel, K., et al., *2D Ti3C2Tx MXene/polyvinylidene fluoride (PVDF) nanocomposites for attenuation of electromagnetic radiation with excellent heat dissipation.* Composites Part A: Applied Science and Manufacturing, 2020. **129**: p. 105693.
8. Niksarlıoğlu, S., et al., *An extensive investigation on gamma shielding properties of PLA/Gd2O3 nanocomposites.* Radiation Physics and Chemistry, 2023. **208**: p. 110936.
9. Ariati, R., et al., *Polydimethylsiloxane composites characterization and its applications: A review.* Polymers, 2021. **13**(23): p. 4258.
10. Liu, J., Y. Yao, X. Li, and Z. Zhang, *Fabrication of advanced polydimethylsiloxane-based functional materials: Bulk modifications and surface functionalizations.* Chemical Engineering Journal, 2021. **408**: p. 127262.
11. Yazdankish, E., *Solving of the Schrodinger equation analytically with an approximated scheme of the Woods–Saxon potential by the systematical method of Nikiforov–Uvarov.* International Journal of Modern Physics E, 2020. **29**(06): p. 2050032.
12. Yazdankish, E. and M. Nejatolahi, *Improved calculation of alpha decay half-life by incorporating nuclei deformation shape and proximity potential.* Physica Scripta, 2023. **98**(11): p. 115309.
13. Yazdankish, E., *Analytical Bound-State solution of the Schrodinger equation for the morse potential within the Nikiforov-Uvarov method.* Mathematics and Computational Sciences, 2021. **2**(1): p. 61-70.
14. Yazdankish, E., *Bound state solution of the Schrodinger equation for the Woods–Saxon potential plus coulomb interaction by Nikiforov–Uvarov and supersymmetric quantum mechanics methods.* International Journal of Modern Physics E, 2021. **30**(04): p. 2150023.
15. Guo, Y., X. Ji, B. Kriesten, and K. Shiells, *Twist-three cross-sections in deeply virtual Compton scattering.* Journal of High Energy Physics, 2022. **2022**(6): p. 1-48.
16. Valdes-Cortez, C., et al., *A study of Type B uncertainties associated with the photoelectric effect in low-energy Monte Carlo simulations.* Physics in Medicine & Biology, 2021. **66**(10): p. 105014.
17. Sirunyan, A.M., et al., *Measurement of top quark pair production in association with a Z boson in proton-proton collisions at s $$\sqrt{\mathrm{s}}$$= 13 TeV.* Journal of High Energy Physics, 2020. **2020**(3): p. 1-50.




[ Downloaded from jgp.yu.ac.ir on 2026-10-05 ]

18. Yazdankish, E., *Calculation of the energy eigenvalues of the Yukawa potential via variation principle.* International Journal of Modern Physics E, 2020. **29**(09): p. 2050067.
19. Erkan, I., A. Yarenoglu, E. Yukseloglu, and H. Ulutin, *The investigation of radiation safety awareness among healthcare workers in an education and research hospital.* International Journal of Radiation Research, 2019. **17**(3): p. 447-453.
20. Gerward, L., N. Guilbert, K.B. Jensen, and H. Levring, *WinXCom—a program for calculating X-ray attenuation coefficients.* Radiation physics and chemistry, 2004. **71**(3-4): p. 653-654.
21. Alkemade, E., *Optimizing Nano-Oscillators*. 2021.
22. Fornalski, K.W., *Simple empirical correction functions to cross sections of the photoelectric effect, Compton scattering, pair and triplet production for carbon radiation shields for intermediate and high photon energies.* Journal of Physics Communications, 2018. **2**(3): p. 035038.
23. Özkalaycı, F., et al., *Lead (II) chloride effects on nuclear shielding capabilities of polymer composites.* Journal of Physics and Chemistry of Solids, 2020. **145**: p. 109543.
24. Issa, S.A. and H. Tekin, *The multiple characterization of gamma, neutron and proton shielding performances of xPbO-(99-x) B2O3–Sm2O3 glass system.* Ceramics International, 2019. **45**(17): p. 23561-23571.
25. Kaçal, M., F. Akman, and M. Sayyed, *Evaluation of gamma-ray and neutron attenuation properties of some polymers.* Nuclear Engineering and Technology, 2019. **51**(3): p. 818-824.
26. Hosamani, M., et al., *Determination of effective atomic number of multifunctional materials using backscattered beta particles–a novel method.* Spectroscopy Letters, 2020. **53**(2): p. 132-139.
27. Tekin, H., et al., *Photon and neutron shielding performance of boron phosphate glasses for diagnostic radiology facilities.* Results in Physics, 2019. **12**: p. 1457-1464.
28. Kaewkhao, J., J. Laopaiboon, and W. Chewpraditkul, *Determination of effective atomic numbers and effective electron densities for Cu/Zn alloy.* Journal of Quantitative Spectroscopy and Radiative Transfer, 2008. **109**(7): p. 1260-1265.
29. Gunoglu, K. and İ. Akkurt, *Radiation shielding properties of concrete containing magnetite.* Progress in Nuclear Energy, 2021. **137**: p. 103776.
30. Sayyed, M., et al., *Physical, structural, optical and gamma radiation shielding properties of borate glasses containing heavy metals (Bi2O3/MoO3).* Journal of Non-Crystalline Solids, 2019. **507**: p. 30-37.
31. Perales-Martínez, I.A., et al., *Enhancement of a magnetorheological PDMS elastomer with carbonyl iron particles.* Polymer Testing, 2017. **57**: p. 78-86.


[ Downloaded from jgp.yu.ac.ir on 2026-10-05 ]